A coastal ocean model intercomparison study for a three-dimensional idealised test case

B. Tartinville [a],[*], E. Deleersnijder [a], P. Lazure [b], R. Proctor [c], K.G. Ruddick [d], R.E. Uittenbogaard [e]

[a] *Institut d'Astronomie et de Géophysique G. Lemaître, Université Catholique de Louvain, 2 Chemin du Cyclotron, B-1348 Louvain-La-Neuve, Belgium*
[b] *IFREMER, Laboratoire d'Hydrodynamique et de Sédimentologie, Centre de Brest, BP-70, F-29280 Plouzané, France*
[c] *Proudman Oceanographic Laboratory, Bidston Observatory, Birkenhead, Merseyside L43 7RA, UK*
[d] *Management Unit of the North Sea Mathematical Models, Gulledelle 100, B-1200 Brussels, Belgium*
[e] *Delft Hydraulics, Rotterdamseweg 185, PO Box 177, 2629 HD Delft, The Netherlands*

Abstract

Several coastal ocean models have been used to compute the circulation on the Northwest European Continental Shelf. Five of them, developed within the European Union, are compared in the scope of an idealised three-dimensional test case, dealing with the geostrophic adjustment of a freshwater cylinder. As the central eddy adjusts, unstable baroclinic vortices start to grow. All the models are able to produce such unstable vortices. However, two of them produce an order-two instability, which is in accordance with a previous laboratory experiment, while the others exhibit an order-four instability. Using a simple scaling analysis, it is seen that the azimuthal wavenumber depends on the ratio of the kinetic energy to the available potential energy. It appears that the discrepancy in the azimuthal wavenumber is mainly due to the effect of the discretisation of the horizontal advection of momentum which could produce significant decrease of the total kinetic energy. © 1998 Elsevier Science Inc. All rights reserved.

Keywords: Model intercomparison; Advection; Baroclinic instability; Geostrophic balance

1. Introduction

Much work has been devoted to the improvement of advection schemes for models of shelf seas (e.g. [1] and references therein), deep ocean (e.g. [2] and references therein), and the atmosphere (e.g. [3] and references therein). In spite of all these efforts, choosing the most appropriate advection scheme for a given geophysical fluid flow problem is still far from trivial. This is why several research programmes are currently addressing this issue [4]. Among them, the NOrth sea Model Advection–Dispersion Study (NOMADS) [5] is concerned with the intercomparison of various advection–dispersion models of the Northwest European Continental Shelf (NECS). In the scope of this study, four realistic test cases dealing with tracer and water transport in the Southern Bight

---

[*] Corresponding author. Tel.: +32 10 47 32 98; fax: +32 10 47 47 22; e-mail: tartin@astr.ucl.ac.be.

of the North Sea have been performed. An additional idealised test case has been carried out and is described in the present article.

The idealised test cases that have been used in previous intercomparison studies [6–8] are either elementary 1D or 2D experiments with analytical solutions or elaborate 3D tests. The former are too simple to produce useful conclusions, while the results of the latter are difficult to interpret. We chose to perform a 3D experiment, simple enough to provide useful conclusions yet relevant to baroclinic processes encountered in reality such as the instabilities and/or frontal meandering associated with many coastal currents [9,10] or isolated eddies [11]. A previously-described numerical experiment [1], which deals with the geostrophic adjustment of a relative freshwater eddy and the development of unstable vortices, meets this requirement. It was found that the shape of the final freshwater core depends on the advection scheme used. Thus, this test case was deemed appropriate for NOMADS.

Five institutions within the European Union have performed the idealised case: the Proudman Oceanographic Laboratory (UK) (PO for short), Delft Hydraulics (NL) (DE for short), the Management Unit of the North Sea Mathematical Models (BE) (MU for short), the Laboratoire d'Hydrodynamique et de Sédimentologie IFREMER (FR) (IF for short) and the Institut d'Astronomie et de Géophysique G. Lemaître (BE) (CL for short). Additional simulations have also been carried out by several participants using various versions of their own model. Those runs gave useful clues to identify the causes of the observed discrepancies.

The present study is one of the first comprehensive intercomparisons, in an idealised test case, of numerous coastal ocean models developed within the European Union. As such, it provides indications concerning the differences which are observed in the realistic simulations. Moreover, it is the first step towards a more elaborate incomparison procedure that should be performed in the future.

2. Model description

Three-dimensional hydrodynamic meso-scale models are used in the present study. Their governing equations express the conservation of mass, momentum and salinity and assume that the Boussinesq approximation and the hydrostatic equilibrium are valid. All the models use the vertical sigma-coordinate. CL, DE, IF and MU models are based on a horizontal C-grid while PO uses a B-grid. Except in DE, the internal and external modes are integrated separately using the mode splitting technique [12]. Furthermore, various numerical schemes for horizontal and vertical advection of salinity and momentum are used. CL uses a Self-Adjusting Hybrid Scheme (SAHS) in the horizontal [13] which, for the salinity, is slightly modified by the addition of an upwinding rate derived from Leith [14]. A first-order upwind scheme is used in the vertical in order to avoid unphysical solutions for the density profile. DE uses a semi-implicit technique in the horizontal with a second-order centred and a higher order (second-order for momentum and third-order for salinity) upwind scheme for the explicit and implicit parts, respectively. A first-order upwind scheme is used for the vertical advection of salinity, while a second-order centred scheme is preferred for the vertical advection of momentum. IF selected the Quickest method for the horizontal and vertical advection of salinity and momentum [15]. MU uses a Total Variation Diminishing (TVD) scheme for the advection of salinity with the Superbee limiting function [16]. A first-order upwind scheme is used for the advection of momentum. PO uses the Piecewise Parabolic Method (PPM) [1] for the advection of salinity and momentum in both directions. The main model characteristics are listed in Table 1, while more detailed descriptions can be found in [1,17,18].

Table 1
Space discretisation of the models used

	Grid	Salinity horizontal advection scheme	Momentum horizontal advection scheme	Salinity vertical advection scheme	Momentum vertical advection scheme
CL	C	SAHS	SAHS	First-order upwind	First-order upwind
DE	C	See text	See text	First-order upwind	Second-order centred
IF	C	Quickest	Quickest	Quickest	Quickest
MU	C	TVD	First-order upwind	TVD	First-order upwind
PO	B	PPM	PPM	PPM	PPM

3. Design of the experiment

All the previous intercomparison studies concluded that the definition of the experiment is of crucial importance. Therefore, special attention is devoted to this point. The present test case is based on that of James [1], which deals with the comparison of advection schemes. Neglecting all forms of mixing in this test case, though unrealistic in terms of oceanic flows, provides a severe test for advection schemes.

The domain is a 20 m deep and 30 km × 30 km open sea region. The latitude is chosen as 52° N and hence the Coriolis parameter is set to 1.15×10^{-4} s^{-1}. The horizontal grid resolution is 1 km and 20 vertical levels are used. In the centre of the domain, a 10 m deep, 3 km radius cylinder of relatively freshwater is placed in the upper layer. The centre of the patch corresponds to the location of a scalar quantity calculated by the model (this is not exactly the centre of the domain: a shift of half a grid box is necessary). The salinity S (in psu) within the eddy is a function of the distance to the centre, d (in km) and is given by

$$S = 1.1 \left[\frac{d}{3} \right]^8 + 33.75. \tag{1}$$

Outside the eddy the ambient salinity is set to 34.85 psu. The state equation for the density, ρ, is linearised as follows:

$$\rho = 1025 + 0.78(S - 33.75). \tag{2}$$

The ambient density and the density at the centre of the patch are thus set to 1025.858 and 1025 kg m^{-3}, respectively. At the beginning of the experiment the water velocity and the sea surface elevation are set to zero. Initial conditions are displayed in Fig. 1. Simulations are performed for 144 h (9.5 inertial periods) without any bottom or surface stress. Vertical and horizontal diffusivity and viscosity are set to zero or minimal values if necessary to avoid numerical instabilities.

The proposed open boundary condition is a four-point-wide relaxation zone [19] for the sea surface elevation and the salinity. Salinity is restored to the ambient value (i.e. 34.85 psu) and elevation is restored to zero, following

$$X = k\hat{X} + (1 - k)\tilde{X}, \tag{3}$$

where $\tilde{X}$ denotes the calculated unrelaxed value, $\hat{X}$ the specified value, X the final value. k is the relaxation parameter, which is specified as a parabolic function equal to 1 at the boundary and then 0.5625, 0.25, 0.0625 and 0.0 inside the domain. The horizontal momentum equation is linearised next to the boundary, so that advection of momentum is not applied there. The relaxation zone is located outside of the 30 × 30 points computational domain. In order to easily perform the test case, the proposed boundary condition is not implemented in DE and MU models. Instead, Riemann-type conditions were used. The effect of this choice will be discussed later.
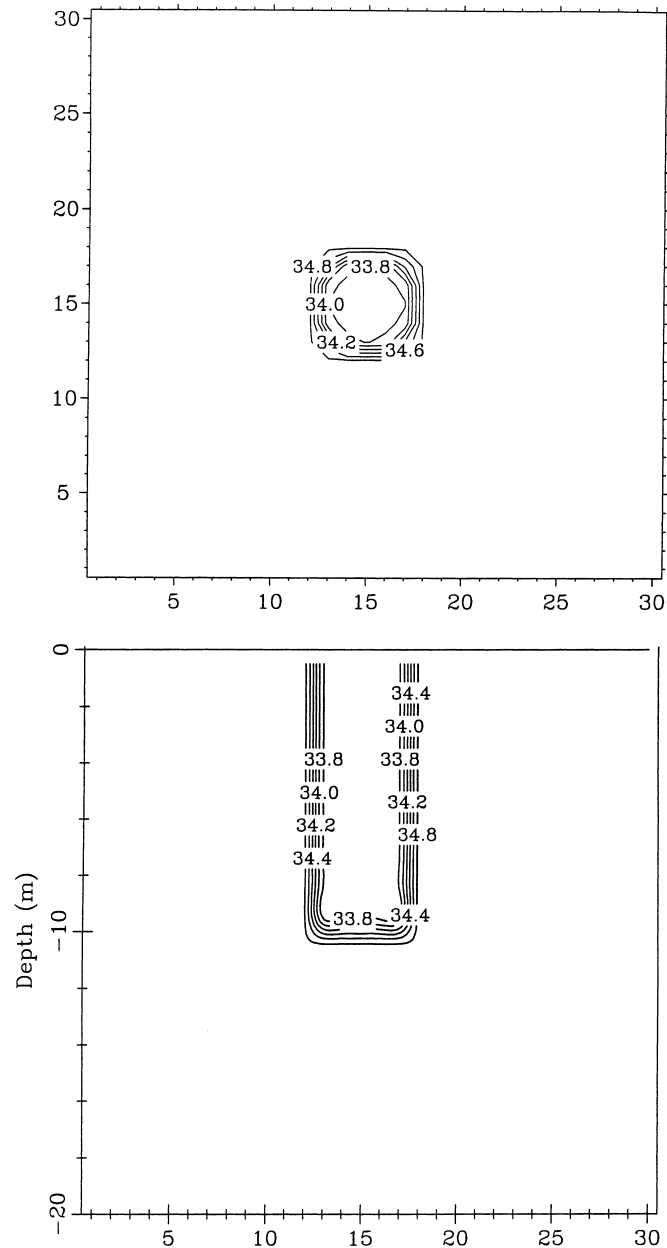
Fig. 1. Initial sea surface salinity (upper panel) and salinity in a vertical section through the centre of the initial fresh-water core (lower panel).

Similar laboratory and numerical experiments have been carried out [1,20–25]. They deal with the geostrophic adjustment of a light/heavy cylindrical core. As it adjusts, the core rises/sinks and spreads out, its available potential energy is converted into kinetic energy and unstable eddies start to grow. According to all those studies, the order of the instability depends on the initial characteristics of the cylinder – i.e. its depth, diameter and density difference with the ambient fluid. It is found that the zonal wavenumber increases if the radius of the initial core increases or the reduced gravity decreases. If the initial cylinder occupies the total water depth, the unstable vortices are generated by baroclinic processes. For example, this phenomenon occurs during the

unstable stage of deep convection [24]. Therefore, the eddies produced are able to transport potential energy away from the initial core. As the initial cylinder depth is reduced, horizontal shear increases and barotropic instabilities are likely to be produced. According to a previous laboratory experiment our test case should produce an order-two mixed barotropic/baroclinic instability (see Fig. 5 from [21]).

4. Model results

All participants provided a set of outputs, which was specified with the experiment definition. This set consists of: timeseries of available potential energy (APe), kinetic energy (Ke) and enstrophy (En) inside the computational domain; the maximum and minimum of salinity (S_{max} and S_{min}) and the surface area (A1%) where salinity is 1% less than the ambient value (i.e. lower than 34.839 psu); and the 3D array of velocities and salinity at the end of the simulation. Numerous data could be added to this set, however too large a number of data would confuse the interpretation. Our prescribed outputs are assumed to be adequate in order to achieve the intercomparison.

Timeseries are displayed in Fig. 2. During the first stage of the experiment, i.e. for times less than one inertial period, surface inertia-gravity waves are created. They radiate outside of the computational domain and induce a rapid decrease of the total energy contained inside the domain [26].

Thereafter, the initial freshwater core tends towards a geostrophically adjusted state. As it adjusts, it pulses inward and outward at a near-inertial frequency. Timeseries of APe, Ke, En and A1% exhibit this near-inertial oscillation. As the core spreads, A1% increases and available potential energy is converted into kinetic energy. As the core contracts, these quantities evolve in the opposite direction. This near-inertial wave is damped by the diffusive properties of the momentum advection schemes. There are large differences between models on the amplitude, the phase and the frequency of this oscillation. The first maximum APe of PO corresponds nearly to the first inertial period, whereas it appears 0.1 inertial periods later for IF.

This wave-like evolution is superimposed on a global spreading of the initial core and a simultaneous conversion of APe into Ke. The total energy stored within the domain during the geostrophic adjustment phase should remain almost constant [22]. While this is valid for most of the models (not shown), DE produces a final decrease of its APe without any similar increase of its Ke, with a consequent decrease in total energy. Furthermore, it appears that the spreading of the initial core varies between models. While PO, MU and DE produce a small spreading, IF and CL exhibit a much larger expansion of their freshwater core. Moreover, while all models produce an almost steady maximum of salinity, very different results are found for the minimum of salinity. MU and PO have a constant S_{min}. DE model slightly under-shoots at the beginning of the experiment and produce a final value of 34.06 psu. CL and IF have an increasing minimum of salinity which reaches a final value of 34.17 and 33.96 psu, respectively.

As the experiment progresses, vortices appear at the edge of the central core and start to grow. The total enstrophy, i.e. the integrated square vorticity, increases as the vortices develop. This instability produces a significant increase of the kinetic energy for PO. It also induces an observed small increase in A1% for all the models. The experiment has not been carried out further in time in order to avoid the significant decrease of the APe that would be caused by the displacement of the vortices out of the computational domain.

At the end of the experiment, all the models exhibit an instability, but the shape of the lobes produced and their number are different. CL produces four well-developed vortices, whereas DE and MU exhibit the same azimuthal wavenumber with less developed eddies (Figs. 3–5). IF and
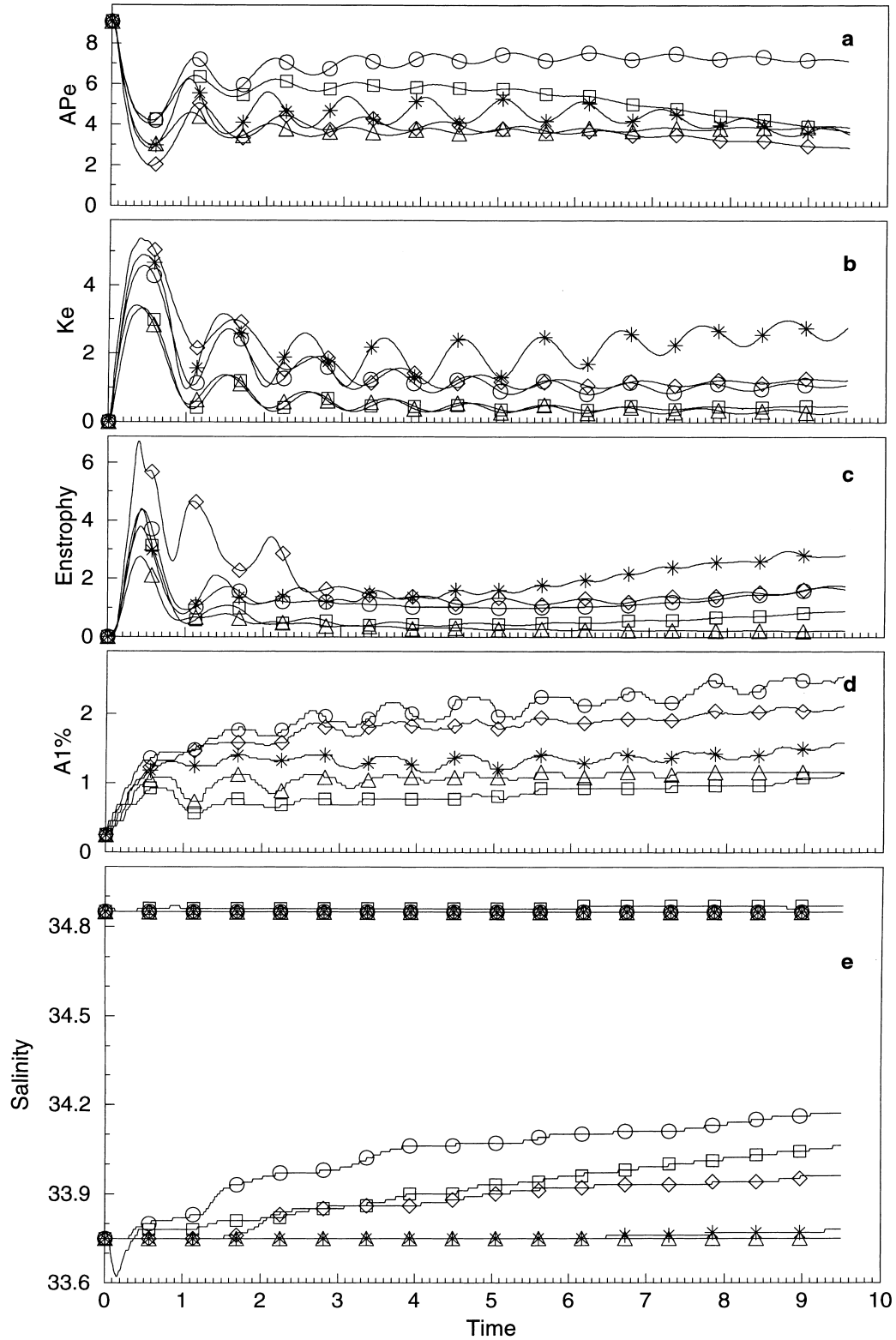
Fig. 2. Timeseries of available potential energy in 10^9 J (a), kinetic energy in 10^9 J (b), enstrophy in $m^3 s^{-2}$ (c), surface area where the salinity is 1% less than the ambiant value in $10^8 m^2$ (d), maximum (e: upper part) and minimum (e: lower part) of salinity in psu. Time is displayed in inertial periods. The curves are labelled with distinguishing symbols, i.e. a circle for CL, a square for DE, a diamond for IF, a triangle for MU and a star for PO.
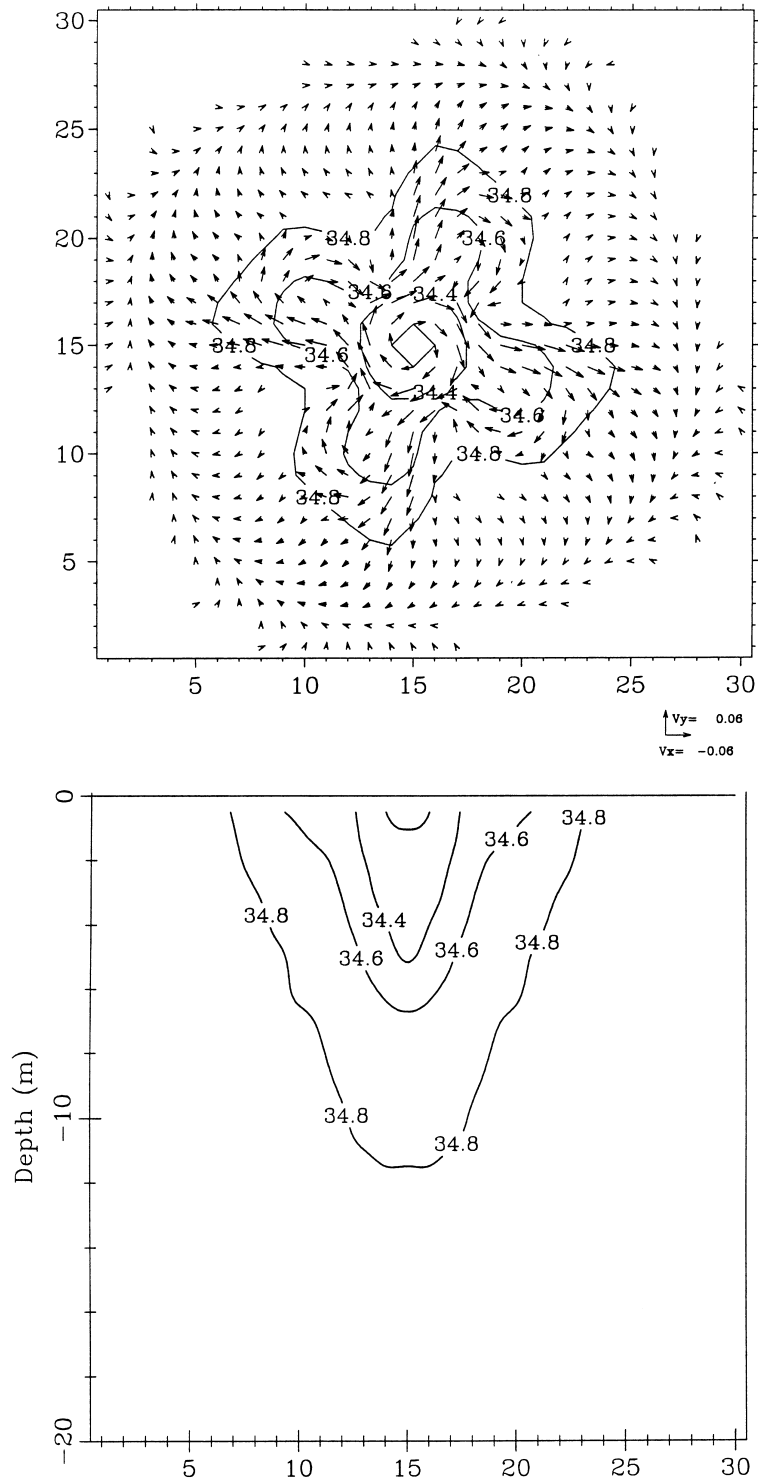
Fig. 3. Sea surface salinity and velocities (upper panel), and salinity in a vertical section through the centre of the central eddy (lower panel) at the end of the CL experiment.
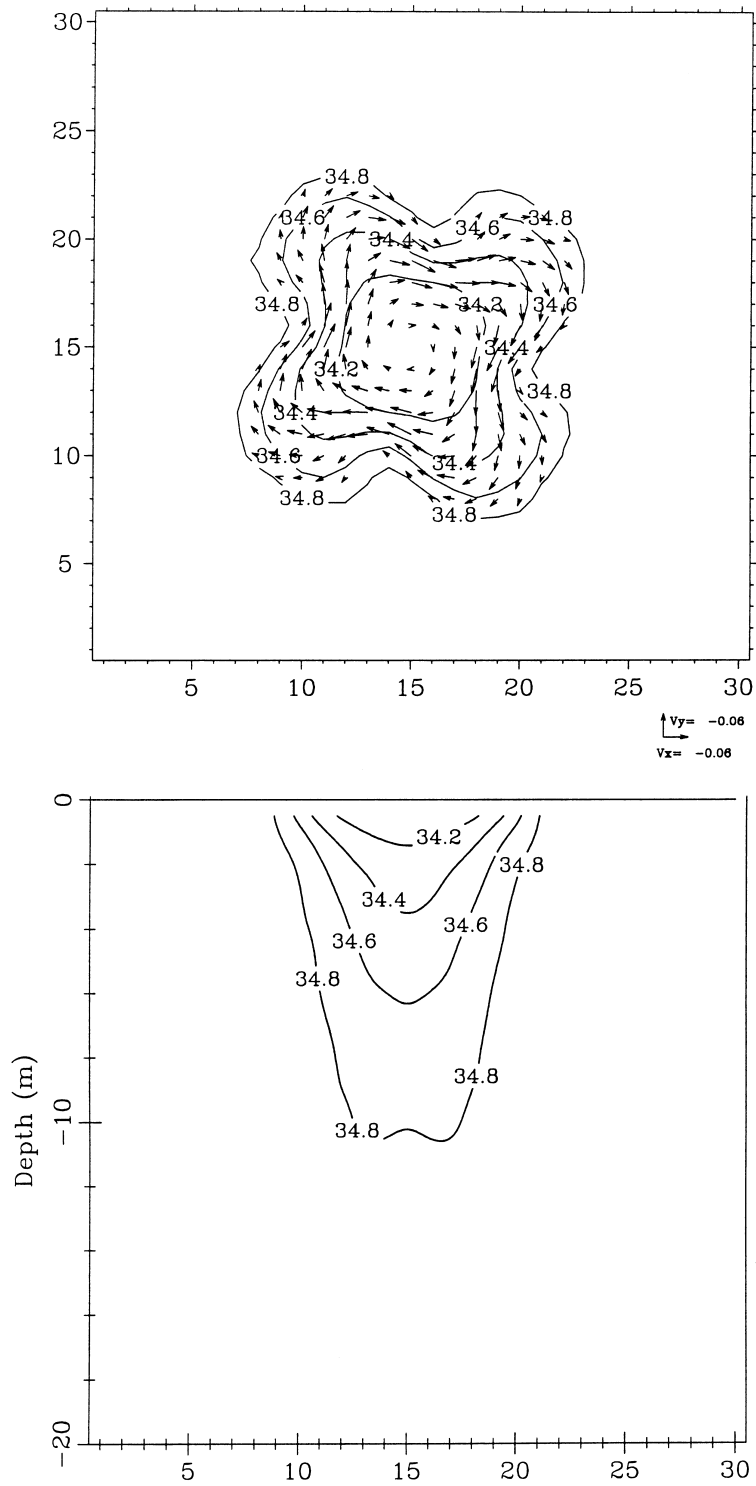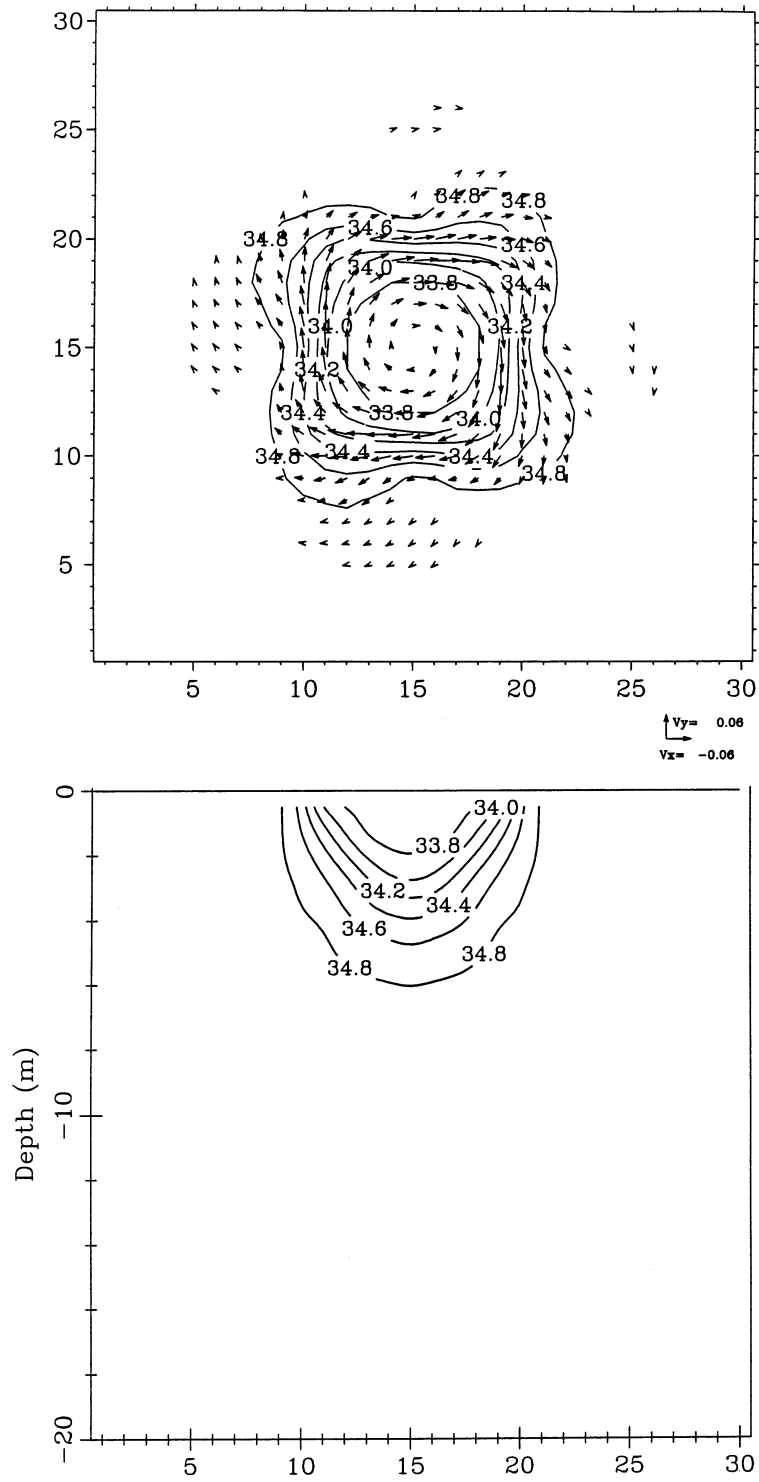
Fig. 4. Same as Fig. 3, for the DE experiment.

Fig. 5. Same as Fig. 3, for the MU experiment.

PO produce an order-two instability, as expected from previous laboratory experiments, but the vortices of the former are less developed than those of the latter (Figs. 6 and 7). In accordance with the geostrophic balance, the surface velocity exhibits a clockwise motion around the freshwater core. Maximum velocities are located at the front of the central eddy (i.e. where the horizontal salinity gradient is maximum). The frontal jet is higher for IF and PO (more than 10 cm s^{-1}) than for the other models (from 4 to 6 cm s^{-1}). This is in agreement with the levels of kinetic energy found at the end of the experiment. Most of the models exhibit alternative upwards and downwards vertical velocities, the magnitude of which is of the order of 10^{-5} m s^{-1}. All models produce a rising and spreading of the less dense core. A salinity less than 33.8 psu is found below 10 m in CL and DE results.

5. Analysis

Unstable waves can be produced by sheared currents. For our test case although previous studies suggest that an order-two mixed barotropic/baroclinic instability should be produced, in practice two different azimuthal wavenumbers were found. In order to understand this discrepancy it seems necessary to look into the properties of the surface vortices and to identify the dominating process which induces the instability.

According to Pedlosky [27], in a cylindrical problem, a less/more dense water core in geostrophic balance should produce baroclinic instabilities if the square of the ratio of its radius to the internal Rossby radius is greater than $\sqrt{2}$. Our experiment meets this requirement.

Moreover, it results from laboratory experiments [20,21] that cyclonic vortices are driven by horizontal shear near the density front. Barotropic processes induce anti-clockwise vortices. On the other hand, surface baroclinic eddies rotate in the same direction as the central eddy, i.e. clockwise. Except PO, all the models exhibit only unstable clockwise surface vortices, i.e. driven by baroclinic processes. Both clockwise and anti-clockwise vortices are found in PO results. This is qualitatively in close agreement with the results of the laboratory experiments.

Both Ke and APe could be separated in two terms. The first represents the energy of the unperturbed geostrophically adjusted state ($\overline{\text{Ke}}$ and $\overline{\text{APe}}$) and the second is its deviation from the equilibrium state (Ke′ and APe′). It follows that

$$\text{Ke} = \overline{\text{Ke}} + \text{Ke}', \tag{4}$$

$$\text{APe} = \overline{\text{APe}} + \text{APe}'. \tag{5}$$

From the classical theory of barotropic instabilities it appears that the growth of the unstable barotropic vortices corresponds to a conversion of $\overline{\text{Ke}}$ into Ke′. On the other hand the development of the baroclinic instability is associated with a corresponding transfer of $\overline{\text{APe}}$ into Ke′ and APe′ [28]. Timeseries from PO, DE and IF show a final increase of their total kinetic energy and a simultaneous decrease of their total available potential energy. Since the APe is converted into Ke as the vortices started to grow, we could assume that there is an increase of Ke′ due to a simultaneous decrease of $\overline{\text{APe}}$.

Therefore, it appears that baroclinic instabilities are likely to be produced, that surface patterns are similar to experimental results dealing with baroclinic processes and that the energy transfer corresponds to the growth of baroclinic eddies. Thus, the models exhibit perturbations which are mainly driven by the baroclinic instability.

Since the unstable vortices are likely to be due to baroclinic processes, a simple scaling analysis may be performed in order to explain the observed discrepancies. Given a freshwater core in geostrophic balance which produces an order-n baroclinic instability, Jones and Marshall [23] sug-
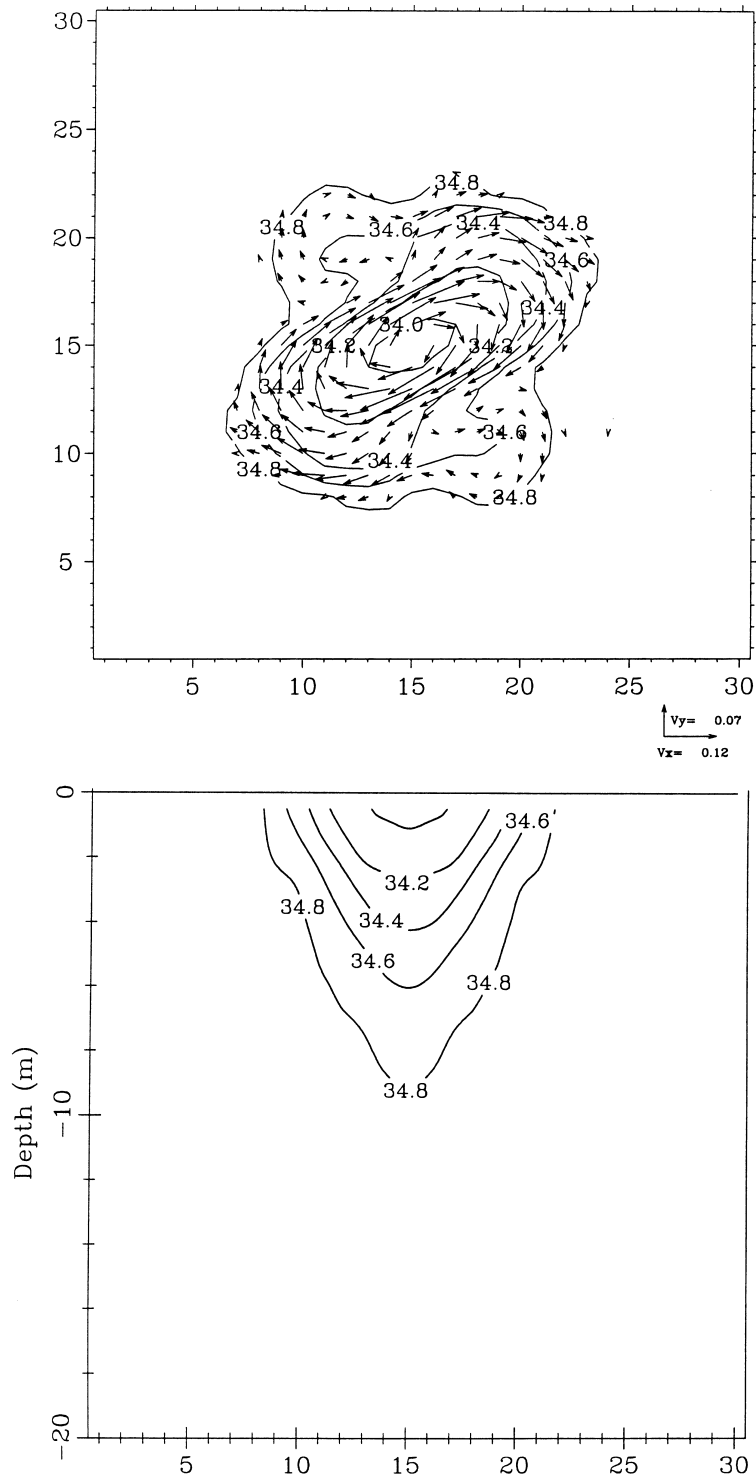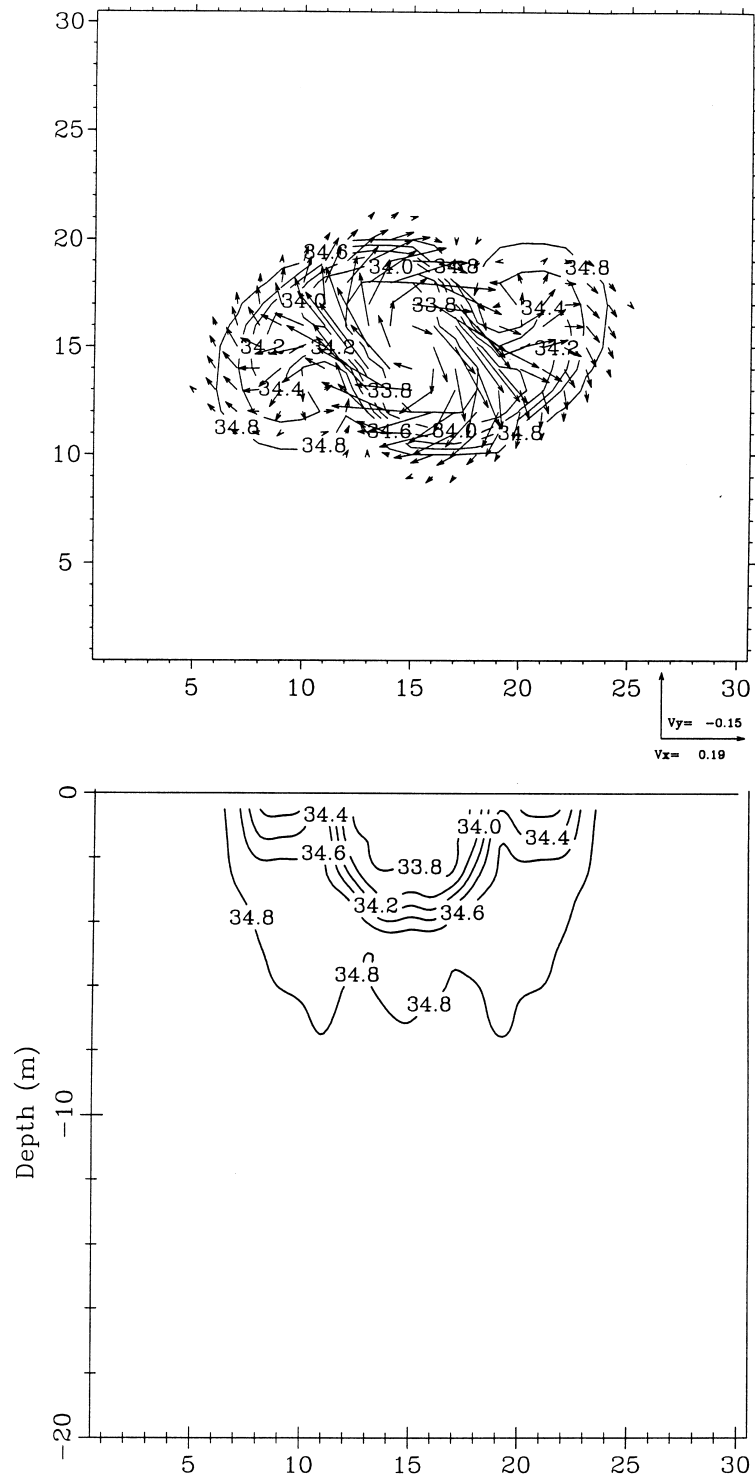
Fig. 6. Same as Fig. 3, for the IF experiment.

Fig. 7. Same as Fig. 3, for the PO experiment.

gest that the radius of the vortices produced, R_v, scales with the internal Rossby radius according to

$$R_v \propto \frac{\sqrt{g'h'}}{f}, \tag{6}$$

where g' denotes the reduced gravity, h' is the characteristic depth of the freshwater core and f the Coriolis parameter. Since unstable lobes are distributed regularly on the perimeter of the central adjusted cylinder, it is assumed that this perimeter L_a scales with R_v as

$$L_a \propto 4nR_v. \tag{7}$$

If R_a denotes the radius of the adjusted freshwater eddy, therefore

$$R_a \propto \frac{2}{\pi} nR_v. \tag{8}$$

Eq. (8) is similar to a previous analytical solution found by Pedlosky [27]. We should further define a velocity scale assuming the geostrophic balance,

$$u \propto \frac{g'h'}{fR_a}. \tag{9}$$

Using Eqs. (6), (8) and (9), it is found that the azimuthal wavenumber scales with the inverse of a Froude number as

$$n \propto \frac{\pi}{2} \frac{\sqrt{g'h'}}{u}. \tag{10}$$

Defining Θ as the ratio of the kinetic energy to the available potential energy in geostrophic balance, it has been demonstrated [29] that

$$\Theta \propto \frac{u^2}{g'h'}. \tag{11}$$

Combining Eqs. (10) and (11) yields

$$n \propto \frac{\pi}{2} \Theta^{-1/2}. \tag{12}$$

Since the steady geostrophically adjusted state is never reached in this experiment, we assume that time-averaged quantities over the duration of the experiment are relevant to the geostrophic equilibrium. Time-averaged Ke, Ape, En and Θ are reported on Table 2. There is a clear relation between the order of the instability and Θ. As suggested by Eq. (12), n increases as Θ decreases. The relationship between those two quantities is displayed in Fig. 8, showing that Eq. (12) is relevant to our experiment and that its scaling factor is close to unity. This suggests that the order of the instability is a function of Ke and APe as the geostrophic balance is reached. Therefore, the discrepancies in the number of vortices is due to a difference in the energy transfer as the initial freshwater core adjusts.

Since the models are in agreement with the baroclinic instability theory, the analysis could be extended in order to explain the discrepancies in the shape of the vortices. According to the classical theory from Eady [30], the growth rate of the most unstable baroclinic mode is

$$\omega = \frac{0.3f}{\sqrt{R_i}}, \tag{13}$$

where R_i is the Richardson number. Since, in geostrophic balance, R_i is the inverse of Θ, using relations (12) and (13) we obtain

Table 2
Time-averaged quantities over the experiment duration and order of the instability

	Ke (10^9 J)	APe (10^9 J)	Θ	Enstrophy (m^3 s^{-2})	n
CL	1.42	6.96	0.22	1.33	4
DE	0.68	5.30	0.13	0.73	4
IF	1.68	3.69	0.50	1.90	2
MU	0.66	3.83	0.18	0.43	4
PO	2.27	4.46	0.55	1.89	2

$$\omega \propto \sqrt{\Theta}. \tag{14}$$

With regard to this equation, comparing two models which produce the same order instability, the one with the highest Θ will show faster growth than the other. This statement is valid for the order-two models: PO has more-developed eddies than IF, and it exhibits the highest Θ. It is also valid for the order-four models: the vortices of DE and MU are smaller than those of CL.

6. Discussion

As stated above, the discrepancies in the number of vortices and their shape could be explained with a simple energy budget argument. Since this test case is intended to compare the numerical methods used, we should go further into the analysis and find the numerical causes of such discrepancies.

Many aspects of the numerical methods used may affect the energy budget. However, some are more important either because they allow the conversion of APe into Ke or because they could introduce an important loss of energy. The overview of the models points to several differences in the numerical methods. Four of them are acceptable candidates. These are the grid-staggering,
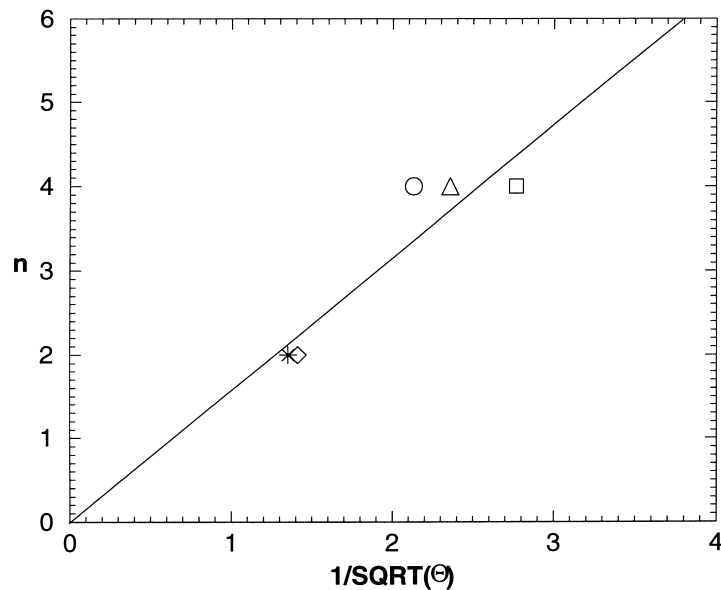

Fig. 8. Relation between the order of the instability and the inverse of the square root of Θ. The symbols used are those described in Fig. 2. The straight line corresponds to Eq. (12).

the open boundary conditions, the salinity advection scheme and the momentum horizontal advection scheme.

Since an interpolation of horizontal velocities is needed to calculate the Coriolis force on a C-grid, a smoother front and a weaker frontal jet is obtained than with a B-grid [31]. Therefore, as in geostrophic balance the Coriolis force balances the horizontal pressure gradient, less energy is transferred from the APe into the Ke and the horizontal arrangement of gridpoints has an impact on the energy budget. In our test case, concerned with geostrophic balance, only PO uses a B-grid. This model produces a wavenumber-two instability and the highest level of kinetic energy. Since most of the kinetic energy is located at the edge of the freshwater core and frontal jets are better represented using a B-grid, this is not surprising. However, an order-two instability is also produced by IF which has a C-grid. Furthermore, an additional test case performed by CL using the B-grid model of Deleersnijder and Campin [32] produces an order-four instability (not shown). Thus, whatever staggered grid is used (B or C) both order-two and order-four instabilities may be found. Additional test cases performed with a refined grid by DE and MU also show an order-four instability, suggesting that the azimuthal wavenumber does not depend critically on the horizontal arrangement of gridpoints.

The flow through the open boundaries is the only external source/sink of energy in our experiment. As described above, the proposed boundary condition is not implemented by all the participants. Two institutes (DE and MU) perform the test case using a radiation type condition instead of the proposed Flow Relaxation Scheme [19]. Both produce an order-four instability. However, CL produces the same azimuthal wavenumber using the proposed boundary condition. Furthermore, if the boundaries are sufficiently far away from the freshwater core they should have little influence on the development of the unstable eddies. Test cases performed by CL with various forms of the computational domain always produce an order-four instability. Since the boundary conditions are dealing with the sea surface elevation at the edge of the computational domain, they have an effect on the outgoing inertia-gravity waves created at the very beginning of the experiment. But, as the total energy should remain constant during the geostrophic adjustment stage, they have almost no effect on the future development of the unstable vortices.

A third candidate is the discretisation of the advection of salinity. Its diffusive properties, which could be more or less important depending on the numerical scheme used, cause a smoother salinity field. In geostrophic balance, this causes a consequent decrease of the Ke. MU uses a very similar TVD scheme to the one used by James [1]. However, an order-four instability is produced by the former while the latter exhibits an order-two instability. Moreover, in [1], where the model used is in fact the model called here PO, it is shown that a wavenumber-two instability is produced whatever salinity advection scheme (TVD or PPM) is used. Therefore, it seems that the salinity advection scheme has no direct influence on the order of the instability.

A fourth candidate is the horizontal advection scheme for momentum. As stated above, its diffusive properties in regions of sharp gradients damp the near-inertial waves and reduce the total kinetic energy. Since the PPM scheme used by PO has a small artificial viscosity [1], its damping is weak and the magnitude of the near-inertial wave remains almost constant (Fig. 2(a) and (b)). These waves are strongly damped by the other models. As stated by Herman and Owens [22] these oscillations may have an influence on the development of the unstable vortices. However, no significant interaction was found in their experiments. As suggested by Tables 1 and 2, two participants (IF and PO), which use high order schemes without any additional viscosity, produce an order-two instability. On the other hand, models with lower order schemes (CL and MU) or an additional kinematic viscosity (DE) create an order-four instability. Therefore, it seems that the order of the instability is closely related to the discretisation of the horizontal advection of momentum. DE performed a test with a first-order upwind scheme instead of the second-order

scheme, as part of the Alternating Direction Implicit procedure, for solving the horizontal momentum equation; it also produced four vortices. MU performed an additional test without any advection of momentum. As for the original experiment an order-four instability started to grow though results were very different because of vigourous undamped vertical motions. An additional experiment using an upstream advection of momentum scheme in IF model, instead of the Quickest scheme, produced four vortices. This is the only test case which produces a different wavenumber than the original version of the model. It proves that the horizontal advection of momentum is of crucial importance. Additional tests with the PO model, in which (a) horizontal viscosity, (b) vertical viscosity and (c) both horizontal and vertical viscosity, were introduced, suggest this is the case, because in each test the tendency to produce order-two instability was decreased.

These results suggest that, among the four candidates that could explain the observed discrepancy in the order of the instability, the momentum horizontal advection scheme seems to be the most consistent. Numerical viscosity could induce a too strong decrease of the kinetic energy within the domain during the adjustment phase. Therefore, as the ratio Θ decreases, an order-four instability is created instead of the expected order-two instability. However, since they have an impact on the energy budget, it is more than likely that the grid staggering and the salinity advection scheme have an impact on the order of the instability, whereas the open boundary condition is of minor importance. As suggested by our experiments, those terms do not have a direct effect but they could interact with the momentum horizontal advection scheme in order to modify the order of the instability, though without any additional tests it is difficult to determine the validity of this statement.

Moreover, several comments should be added to this discussion. An obvious finding is that none of the models produces an odd-order instability. This is somewhat surprising: since both order-two and order-four instabilities are found, and in accordance with Eq. (12), an order-three instability is to be expected for an adequate range of the parameter Θ. In so far as the initial problem is axisymmetric, as a square grid is used and as the models should conserve symmetry, models seem to be unable to produce such an instability without a mode-three external azimuthal forcing. However, since the noise in laboratory experiments is much more pronounced than in numerical experiments, odd-order instabilities are found in the laboratory experiments [20,21].

A second additional finding concerns the numerical scheme used for the vertical advection of salinity. Two participants (CL and DE) have performed the test case with a first-order upwind scheme, whereas the others use an higher order and less diffuse scheme. This former simple technique is chosen in order to avoid unacceptable behaviours such as an over-shooting or wiggles on the salinity profile caused by the centred scheme. Thanks to the properties of the numerical scheme used, those models produce a very diffusive freshwater core. As the vertical numerical diffusion becomes significant, freshwater parcels are displaced downwards, smoothing the salinity profile and increasing the APe. This is closely related to the findings of Table 2, where CL and DE have the highest APe.

7. Conclusion

This article describes an intercomparison study of five coastal ocean models dealing with a three-dimensional test case. It appears that the order of the baroclinic instability produced depends on the energy budget during the adjustment phase. From a numerical point of view, the discrepancy in the azimuthal wavenumber is attributed to a difference in the scheme for horizontal advection of momentum. Low-order schemes or schemes with an additional viscosity which dis-

sipate kinetic energy produce four vortices, whereas higher order schemes produce two lobes. The practical implication is that the numerical modelling of low-diffusion marine systems where frontal instability processes are important requires the use of at least a second-order discretisation for the advection of momentum. Therefore a special attention should be devoted to this point in numerical applications related to those processes. The relevance of this conclusion for real applications depends, of course, on the existence and importance of processes involving advection of momentum. Examples of such situations will include the meandering of river plume fronts or coastal currents or, more generally, baroclinic instability in an oceanic frontal system. In such cases use of low-order scheme for the advection of momentum can expected to seriously degrade results.

Intercomparison techniques have never been carefully studied. Most of the previous intercomparisons of coastal ocean models led to rather unconclusive results, usually because the test cases were ill-defined or too simple. Our test case was set-up following a previously published study [1] and outputs were chosen with careful forethought. As a result, conclusive remarks can be produced and it is found that the choice of the test case is of crucial importance in order to achieve the intercomparison. However, it is believed that work is still needed in order to improve the intercomparison methods.

Acknowledgements

References

[1] I.D. James, Advection schemes for shelf sea models, J. Mar. Sys. 8 (1996) 237–254.

[2] R. Gerdes, C. Koberle, J. Willebrand, The influence of numerical advection schemes on the results of ocean general circulation models, Climate Dynamics 5 (1991) 211–226.

[3] R.B. Rood, Numerical advection algorithms and their role in atmospheric transport and chemistry models, Rev. Geophys. 25 (1) (1987) 71–100.

[4] J.M. Beckers et al., MEDiterranean Models Evaluation eXperiment (MEDMEX), in: Proceedings of Second MAST days Conference, 1995, pp. 42–52.

[5] R. Proctor et al., EC concerted action in the field of numerical modelling of marine systems, NOMADS-North sea Model Advection Dispersion Study, Final Report, POL International Document No. 108, 1997, 55 pp.

[6] A.M. Baptista, E.E. Adams, P. Gresho, Benchmark for the transport equations: The convection–diffusion forum and beyond, in: D.R. Lynch, A.M. Davies (Eds.), Quantitative Skill Assessment for Coastal Ocean Models, American Geophysical Union, 47, Washington DC, 1995, pp. 241–268.

[7] L.P. Røed et al., A review of the metocean modeling project (MOMOP) Part 1: Model comparison study, in: D.R. Lynch, A.M. Davies (Eds.), Quantitative Skill Assessment for Coastal Ocean Models, American Geophysical Union, 47, Washington DC, 1995, pp. 285–305.

[8] B. Hackett et al., A review of the metocean modeling project (MOMOP) Part 2: Model validation study, in: D.R. Lynch, A.M. Davies (Eds.), Quantitative Skill Assessment for Coastal Ocean Models, American Geophysical Union, 47, Washington DC, 1995, pp. 307–327.

[9] J.M. De Kok, Baroclinic eddy formation in a Rhine plume model, J. Mar. Sys. 12 (1997) 35–52.

[10] V.H. Kourafalou et al., The fate of river discharge on the continental shelf. I. Modeling the river plume and the inner shelf coastal current, J. Geophys. Res. 101 (C2) 3415–3434.

[11] H. Legg et al., A heton perspective of baroclinic eddy transfer in open ocean convection, J. Phys. Oceanogr. 26 (1996) 2251–2266.

[12] A. Blumberg, G. Mellor, A description of a three-dimensional coastal ocean circulation model, in: N.S. Heaps (Ed.), Three-Dimensional Coastal Ocean Models, American Geophysical Union, Washington DC, 1987, pp. 1–16.

[13] A. Harten, The artificial compression method for computation of shocks and contact discontinuities: III. Self-adjusting hybrid schemes, Math. Comput. 32 (1978) 363–389.

[14] C.E. Leith, Numerical simulation of the Earth's atmosphere, Methods Comput. Phys. 4 (1965) 1–28.

[15] B.P. Leonard, A stable and accurate convective modelling procedure based on quadratic upstream interpolation, Comput. Methods Appl. Mec. Eng. 19 (1979) 59–98.

[16] P.L. Roe, Some contribution to the modelling of discontinuous flows, in: Proceedings of 1983 AMS–SIAM Summer Seminar on Large Scale Computing in Fluid Mechanics, Lectures in Applied Mathematics, vol. 22, SIAM, Philadelphia, 1985, pp. 163–193.

[17] K.G. Ruddick, Modelling of Coastal Processes Influenced by the Freshwater Discharge of the Rhine, Ph.D. Dissertation, Université de Liège, Faculté des Sciences, 1995, 247 pp.

[18] B. Tartinville, E. Deleersnijder, J. Rancher, The water residence time in the Mururoa atoll lagoon: Sensitivity analysis of a three-dimensional model, Coral Reefs 16 (1997) 193–203.

[19] E.A. Martinsen, H. Engedahl, Implementation and testing of a lateral boundary scheme as an open boundary condition in a barotropic ocean model, Coastal Eng. 11 (1987) 603–627.

[20] P.M. Saunders, The instability of baroclinic vortex, J. Phys. Oceanogr. 3 (1973) 61–65.

[21] R.W. Griffiths, P.F. Linden, The stability of vortices in a rotating, stratified fluid, J. Fluid Mech. 105 (1981) 283–316.

[22] A.J. Hermann, W.B. Owens, Modeling the geostrophic adjustment and spreading of waters formed by deep convection, in: P.C. Chu, J.C. Gascard (Eds.), Deep Convection and Deep Water Formation in the Oceans, Elsevier Oceanographic Series, vol. 57, Amsterdam, 1991, pp. 283–308.

[23] H. Jones, J. Marshall, Convection with rotation in neutral ocean: A study of open-ocean deep convection, J. Phys. Oceanogr. 23 (1993) 1009–1039.

[24] U. Send, J. Marshall, Integral effects of deep convection, J. Phys. Oceanogr. 25 (1995) 855–872.

[25] M. Visbeck, J. Marshall, H. Jones, Dynamics of isolated convective regions in the ocean, J. Phys. Oceanogr. 26 (1996) 1721–1734.

[26] J.F. Middleton, Energetics of linear geostrophic adjustment, J. Phys. Oceanogr. 17 (1987) 735–740.

[27] J. Pedlosky, The instability of continuous heton clouds, J. Atmos. Sci. 42 (14) (1985) 1477–1486.

[28] P.H. LeBlond, L.A. Mysak, Waves in the Ocean, Elsevier Oceanography Series, Amsterdam, 1989, 602 pp.

[29] B. Cushman-Roisin, Introduction to Geophysical Fluid Dynamics, Prentice-Hall, London, 1994, 320 pp.

[30] E.T. Eady, Long waves and cyclone waves, Tellus 1 (1949) 33–52.

[31] A.J. Semtner, History and methodology of modelling the circulation of the world ocean, in: J.J. O'Brien (Ed.), Advanced Physical Oceanographic Numerical Modelling, NATO ASI Series, 1986, pp. 23–32.

[32] E. Deleersnijder, J.-M. Campin, On the computation of the barotropic mode of a free-surface world ocean model, Ann. Geophys. 13 (1995) 675–688.